An invariant based transversely-isotropic constitutive model for unidirectional fibre reinforced composites considering the matrix viscous effects

P.-W. GERBAUD[a,b], F. OTERO[b,c], P. BUSSETTA[b,d], P. P. CAMANHO[b,e,*]

[a]*ENS Cachan, Université Paris-Saclay, Av. du Président Wilson 61, Cachan 94235, France*
[b]*INEGI, Rua Dr. Roberto Frias, Porto 4200-465, Portugal*
[c]*CIMNE, Gran Capita s/n 08034, Barcelona, Spain*
[d]*Michelin, Technology centre, Ladoux, 63040 Clermont-Ferrand cedex 9,France*
[e]*DEMec, Faculdade de Engenharia, Universidade do Porto Rua Dr. Roberto Frias, Porto 4200-465,Portugal*

Abstract

Fibres Reinforced Polymers (FRPs) are found in several applications in aeronautics, space and in the automotive industry. These applications are exposed to loading conditions, including impact, which results in a complex mechanical response that is vital to accurately predict. This is particularly important for a new generation of thermoplastic-based composites. The model proposed in this work is an invariant-based approach to represent viscous effects in polymer composites. The model developed only requires two viscous parameters to calibrate the viscoelastic behaviour. A good correlation between the simulations and experimental data obtained in off-axis tests in tension and compression is obtained.

Keywords: Constitutive model, Fibre reinforced polymers, Viscoplasticity, Viscoelasticity, Invariant theory

*Corresponding author.
Email address: pcamanho@fe.up.pt (P. P. CAMANHO)

1. Introduction

1.1. Context

Initially found mostly in leading technological sectors like aeronautics and space, the number of applications in which Fibres Reinforced Polymers (FRPs) are used, as well as the diversity of these applications, are increasing. Along with it, there is the necessity to accurately predict the behaviour of composite structures under various loading scenarios. Furthermore, carbon-epoxy systems are currently widespread but thermoplastic composites are likely to be the next main composite system used, especially in the automotive industry. It is also noted that composite structures may be subjected to high-speed loading cases. Some examples are bird or hail impact, tire explosion and crash events. Taking into account that, in general, both thermoplastic and thermoset matrix based composite present a viscous behaviour, strain rate effects must be captured by advanced constitutive models. Such models enable a reduction of safety factors when designing new parts, and enable the use of less material, which results in weight savings. Due to the complexity of the material, two different types of numerical model can be considered: a micro-scale model – the fibre, interface and the matrix behaviour are explicitly modelled, or an equivalent homogeneous material. The micro-scale model is more expensive from a numerical point of view, but the definition of the equivalent material model can be arduous and may require many material parameters. The objective of this work is to define and validate a homogeneous material law at the ply level for UniDirectional (UD) fibre reinforced polymers that takes into account viscous effects in both the elastic and inelastic deformation regimes.

1.2. State of the art

Due to their attractive mechanical properties, rapid processing and relatively low manufacturing cost, thermoplastic polymer composites represent a promising alternative to thermoset based composites for aerospace and automotive applications. This is not a recent finding as studies were already led back in the 90's. For example, Jar and Kausch (1994) investigated the influence of moulding conditions on the delamination behaviour of carbon-fibre/PEEK composites in 1994. It appeared that the cooling rate and the forming temperature have an impact on the delamination resistance. Indeed, in order to form better quality laminates, a higher forming temperature and a slower cooling rate are needed, which led to increased production costs. Other studies, like that from Gao and Kim (2000), also investigated the cooling rate effect and arrived to the same conclusions. These studies improved the understanding of the material composition and provided additional basis to develop more accurate constitutive models.

The behaviour of thermoplastic polymers is rather complex as it is time, strain rate and temperature dependent, coupling both the viscoelastic and viscoplastic modes of deformation. El-Qoubaa and Othman (2015, 2016) investigated the yield stress of PEEK for different temperatures and strain rates. These studies reveal that the yield stress of PEEK depends on the strain rate and also on the temperature. El-Qoubaa and Othman (2015, 2016) work also covers the glass transition of the material which induces important changes in the material properties. Rae et al. (2007) work on the mechanical properties of PEEK clearly demonstrated viscous effects in the mechanical response of the PEEK in both the elastic and plastic regimes. The model for the matrix developed by Garcia-Gonzalez et al. (2017), calibrated with Rae et al.'s work, takes this phenomenon into account but

was developed for the neat resin, not for composite materials. Therefore, models for the prediction of the behaviour of thermoplastic composites should account for these viscous effects in the elastic and plastic domains.

Vogler et al. (2013) developed an elastic-plastic model capable of predicting the behaviour of UD plies of FRPs with good accuracy. However this model did not account for the viscous effects. This model relies on the invariant theory, which is mathematical framework that enables the representation of anisotropy using isotropic tensorial functions. Hence, using such framework, the formulation can be the same regardless of the orientation angle of the fibres. Currently, the available constitutive models capable of predicting the material response prior to cracking in FRPs laminates include those proposed by Vaziri et al. (1991), Gates and Sun (1991) or Chen and Sun (1993) in the 90's.

Vaziri et al. (1991)'s work aims to address nonlinear behaviour up to and including the failure of single layers of a laminate composite. It is derived within the framework of rate-independent theory of orthotropic plasticity. A quadratic criterion for the plastic yield is used, and the plastic surface is assumed to be similar in tension or compression. The criterion is different depending on, whether the material is UD or BiDirectional (BD). The Tsai-Hill criterion is used for the UD case, along with an associated flow rule. That model does not take into account the viscous effect but it is very efficient compared to more complex constitutive models.

Chen and Sun (1993) proposed a quadratic plastic potential associated with an isotropic hardening. This potential must meet the orthotropic symmetry, and an associated flow rule was used. The necessary elastic constants to formulate the potential were determined using a micro-mechanical model based on an RVE.

The plastic potential uses four parameters, but viscous effects are not accounted for.

Gates and Sun (1991) use the elastic/plastic flow rule presented by Sun and Chen (1989). In order to account for the viscoplasticity, the authors assume an additive decomposition of the elastic and the plastic part of the strain rate. The Perzyna (Perzyna (1963)) overstress function was used to express the plastic strain rate. A power law expression using two parameters to link the effective plastic strain rate and the overstress was also used. This simple model can accurately predict the behaviour of graphite/thermoplastic composites, with few parameters that can easily be obtained via tensile tests. The model does not account for the viscous effect in the elastic domain and the orientation of the specimen must be carefully controlled in the identification of the properties used in the model.

The predictive capabilities of the models described in the previous points are summarised in Tab. 1. It is clear that there is the need to continue the development of constitutive models in order to fully determine the rate-dependent stress-strain response prior to cracking, and to prepare the arrival of the next generation of thermoplastic composites where pre-locatization non-linearities are likely to play an important role in the material/structural performance.

1.3. Modelling strategy proposed

Following an experimental investigation of the Hexcel® IM7-8552 (carbon/epoxy) material system (Koerber et al. (2010); Kuhn et al. (2015)), the importance of the viscous effects in the material system were clearly highlighted. The model proposed by Vogler et al. (2015) was first upgraded to take into account the observed viscous behaviour for high strain-rates in the plastic response (Vogler et al. (2015); Koerber et al. (2018)). In order to calibrate that model, scaling functions were

Model elastic-plastic	Viscoelastic	Viscoplastic	Orientation independent
Sun and Chen (1989)	–	–	–
Vaziri et al. (1991)	–	–	–
Gates and Sun (1991)	–	X	–
Chen and Sun (1993)	–	–	–
Vogler et al. (2013)	–	–	X
Koerber et al. (2018)	–	X	X

Table 1: Behaviour addressed by the reviewed models.

used to model the experimentally observed viscoelastic behaviour. This solution is very limited and a better formulation in the framework of the invariant theory is required.

Based on the previous work (Gerbaud et al. (2018)), the objective of this paper is to present a new fully three-dimensional transversely isotropic viscoelastic-viscoplastic model for FRPs laminates. This model is capable of predicting accurately the viscous effects and the non-linearities in the material response prior to the onset of cracking. It can be further calibrated for the next generation of thermoplastic composites. The proposed model is implemented in a user material subroutine using an explicit formulation in the finite element commercial software package Abaqus/Explicit (Dassault Systèmes). The available tension and compression tests are simulated using a VUMAT user subroutine.

1.4. Outline of the paper

Firstly, the constitutive model formulated in the framework of the invariant theory is presented. The material calibration is discussed, followed by a comparison between the numerical and experimental results. The efficiency of the model proposed, in term of computing time and ability to correctly predict the viscous effects, as well as its comparison with the old versions are investigated. Finally, the main conclusions of the work conducted are presented.

2. Constitutive model

2.1. Invariant based transversely-isotropic formulation

The constitutive model originally proposed by Vogler et al. (2013), is further developed here by including a viscous extension to the original elastic-plastic model. The small deformation theory is used to formulate the model, therefore, the following strain additive decomposition is assumed

$$\boldsymbol{\varepsilon} = \boldsymbol{\varepsilon}_{\text{ve}} + \boldsymbol{\varepsilon}_{\text{vp}}, \tag{1}$$

where -ve- stands for "viscoelastic" and -vp- for "viscoplastic", while $\boldsymbol{\varepsilon}$ represents the total strain.

A structural tensor $\boldsymbol{A}$ that represents the symmetry conditions of transversely isotropic materials is defined by the dyadic product of the unit vector of the preferred (fibre) direction $\underline{a}$ as

$$\boldsymbol{A} = \underline{a} \otimes \underline{a}. \tag{2}$$

The use of such as structural tensor enables a formulation of the anisotropy free of any reference coordinate system. Therefore, the material symmetries are viewed

as an intrinsic material property and, the structural tensor is an additional argument in the constitutive equations.

Following Vogler et al. (2013), the structural tensor is used as an additional argument in order to formulate the elastic free energy density, the yield function and the plastic potential formulation. In the model proposed here, $\boldsymbol{A}$ is used in the formulation of the viscoplastic creep function, the viscoplastic potential and the viscoelastic model. The elastic free energy density for the proposed transversely isotropic model reads

$$\begin{aligned}\Psi(\boldsymbol{\varepsilon}, \boldsymbol{A}) \coloneqq \frac{1}{2}\lambda[\mathrm{tr}(\boldsymbol{\varepsilon})]^2 + \mu_T \mathrm{tr}(\boldsymbol{\varepsilon}^2) + \alpha(\underline{a}\boldsymbol{\varepsilon}\underline{a})\mathrm{tr}(\boldsymbol{\varepsilon}) \\ + 2(\mu_L - \mu_T)(\underline{a}\boldsymbol{\varepsilon}^2\underline{a}) + \frac{1}{2}\beta(\underline{a}\boldsymbol{\varepsilon}\underline{a})^2,\end{aligned} \tag{3}$$

with the five elasticity constants λ, μ_T, μ_L, α, β as invariant coefficients.

The stress tensor $\boldsymbol{\sigma}$ and the elasticity tensor $\mathbb{C}_e$ can be obtained by computing the first and the second derivatives of the free energy density with respect to the strain tensor, respectively:

$$\boldsymbol{\sigma} = \partial_{\boldsymbol{\varepsilon}}\Psi(\boldsymbol{\varepsilon}, \boldsymbol{A}) \quad , \quad \mathbb{C}_e = \partial^2_{\boldsymbol{\varepsilon}\boldsymbol{\varepsilon}}\Psi(\boldsymbol{\varepsilon}, \boldsymbol{A}). \tag{4}$$

2.2. Transversely-isotropic viscoelastic formulation

The viscoelastic extension implemented is based on the model proposed by Kaliske and Rothert (1997) and Kaliske (2000). This model is based on generalised Maxwell model as can be seen in Fig. 1. In this model, there is one main branch, with index 0, corresponding to one linear spring. The elastic modulus C_0 is the original elastic modulus or quasi-static material property. There is another branch in parallel, with index 1, which consists of one Maxwell element, characterised by its elastic modulus C_1 and its relaxation time τ_1. The equations

for the one-dimensional rheological model are presented hereafter, afterwards a generalisation to a fully 3D formulation is shown.

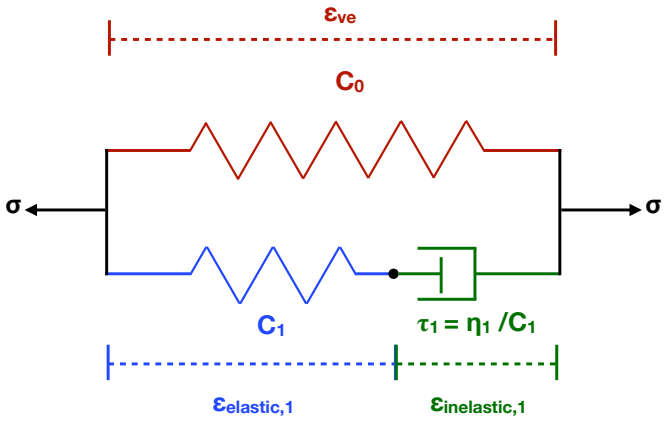

Figure 1: Schematic representation of the generalised 1D viscoelastic Maxwell model.

The total stress can be decomposed as:

$$\sigma = \sigma_0 + \sigma_1, \tag{5}$$

with

$$\sigma_0 = C_0\, \varepsilon_{\text{ve}} \qquad \text{and} \qquad \sigma_1 = C_1\, \varepsilon_{\text{elastic},1} = C_1\, \tau_1\, \dot{\varepsilon}_{\text{inelastic},1}. \tag{6}$$

The strains are calculated as:

$$\varepsilon_{\text{ve}} = \varepsilon_{\text{elastic},1} + \varepsilon_{\text{inelastic},1}, \tag{7}$$

The differential equation for the stress in the one Maxwell element model is therefore calculated as:

$$\Gamma_1 \, \dot{\sigma_0} = \dot{\sigma_1} + \frac{1}{\tau_1} \, \sigma_1, \tag{8}$$

where $\Gamma_1 = C_1 C_0^{-1}$. The analytical solution of the previous equation reads:

$$\sigma_1(t) = \int_0^t \Gamma_1 \, e^{\left(-\frac{t-t^*}{\tau_1}\right)} \, \frac{\partial \sigma_0}{\partial t^*} \, dt^*. \tag{9}$$

In a incremental-iterative time scheme numerical solution, at $t = t_{n+1}$ and by assuming a linear evolution of the stress σ_0 between t_{n+1} and t_n , with $\Delta t^{n+1} = t^{n+1} - t^n$, an approximation of the solution can be obtained

$$\sigma_1^{n+1} \simeq f_1^{n+1} \sigma_1^n + f_2^{n+1} \, \Gamma_1 \, (\sigma_0^{n+1} - \sigma_0^n), \tag{10}$$

where

$$f_1^{n+1} = e^{(-\Delta t^{n+1}/\tau_1)}, \quad \text{and} \quad f_2^{n+1} = \frac{1 - e^{(-\Delta t^{n+1}/\tau_1)}}{\Delta t^{n+1}/\tau_1}. \tag{11}$$

With Eq. (10) it is possible to fully determine the stresses at a given time step $n+1$ using the previous stresses, i.e. σ_1^n and σ_0^n. Only the stresses in the branch 1 depend on the strain rate.

The same equations can be implemented for the 3D scenario, however, additional experimental data is necessary to determine the relaxation times in every direction. Poon and Ahmad (1998) have proposed a relaxation time tensor, using relaxation times close to each other for each direction. In Poon and Ahmad (1998)'s work, the characteristic relaxation time tensor, i.e. $\mathbb{T}_1$, was defined as:

$$\mathbb{T}_1 = \tau_1 \mathbb{I}, \tag{12}$$

where $\mathbb{I}$ is the fourth order unit tensor defined as $I_{ijkl} = \delta_{ik}\delta_{jl}$. This choice simplifies the model formulation by using only one characteristic relaxation time parameter for every direction. Therefore, the system of equations for the 3D formulation is the following:

$$\begin{aligned} \boldsymbol{\sigma}_0^{n+1} &= \boldsymbol{\sigma}_0^n + \mathbb{C}_0 : \Delta\boldsymbol{\varepsilon}_{\text{ve}}^{n+1}, \\ \boldsymbol{\sigma}_1^{n+1} &= f_1^{n+1}\,\boldsymbol{\sigma}_1^n + \; f_2^{n+1}\,\mathbb{\Gamma}_1 : \mathbb{C}_0 : \Delta\boldsymbol{\varepsilon}_{\text{ve}}^{n+1}, \\ \boldsymbol{\sigma}^{n+1} &= \boldsymbol{\sigma}_0^{n+1} + \boldsymbol{\sigma}_1^{n+1}. \end{aligned} \tag{13}$$

The viscoelastic prediction is now expressed in terms of the predicted stress $\boldsymbol{\sigma}^{\text{pred},n+1}$ as

$$\begin{cases} \boldsymbol{\varepsilon}^{n+1} &= \boldsymbol{\varepsilon}_{\text{ve}}^{n+1}, \\ \boldsymbol{\sigma}^{\text{pred},n+1} &= \boldsymbol{\sigma}_0^n + f_1^{n+1}\boldsymbol{\sigma}_1^n + \mathbb{C}_{\text{ve}}^{n+1} : \Delta\boldsymbol{\varepsilon}^{n+1}, \end{cases} \tag{14}$$

with

$$\mathbb{C}_{\text{ve}}^{n+1} = [\mathbb{I} + f_2^{n+1}\mathbb{\Gamma}_1] : \mathbb{C}_0. \tag{15}$$

The fourth order tensor $\mathbb{\Gamma}_1$, or $\hat{\boldsymbol{\Gamma}}$ using Voigt notation, for a transverse isotropic material in the material coordinate system, where the fibres direction coincides with direction 1, can be written as

$$\hat{\boldsymbol{\Gamma}} = \begin{bmatrix} \gamma_{11} & \gamma_{12} & \gamma_{12} & 0 & 0 & 0 \\ \gamma_{21} & \gamma_{22} & \gamma_{23} & 0 & 0 & 0 \\ \gamma_{21} & \gamma_{23} & \gamma_{22} & 0 & 0 & 0 \\ 0 & 0 & 0 & \gamma_{44} & 0 & 0 \\ 0 & 0 & 0 & 0 & \gamma_{44} & 0 \\ 0 & 0 & 0 & 0 & 0 & \gamma_{66} \end{bmatrix}. \tag{16}$$

There are different methods to determine $\mathbb{\Gamma}_1$ in the correct coordinate system. As an example, each component of $\mathbb{\Gamma}_1$ can be computed after defining each component of $\mathbb{C}_1$ and apply $\mathbb{\Gamma}_1 = \mathbb{C}_1 : \mathbb{C}_0^{-1}$. Once the independent parameters, which can be up to seven, of this fourth order tensor in the material coordinate system are known, the tensor can be transformed into a matrix using Voigt notation, the matrix can be rotated in the current coordinate system and finally be rewritten as a fourth order tensor in the current coordinate system. This approach is complicated because all the parameters must be calibrated. Moreover, the rotation is computationally expensive and it may compromise the accuracy of the numerical model.

2.3. Proposed invariant based viscoelastic-viscoplastic formulation

The presented work includes a viscoelastic extension to the viscoplastic model proposed by Vogler et al. (2015) and Koerber et al. (2018). In the later model, similarly to the plastic formulation, a decomposition of the stress state in "viscoplasticity inducing" stresses and assumed "elastic reaction" stresses was used. The "viscoplasticity inducing" part of the stresses has an influence on the viscoplastic behaviour, i.e. on the plastic yield and viscoplastic evolution, and it is used further in the formulation of the viscoplastic creep surface. The "elastic reaction" part of the stresses plays no role in the viscoplasticity. Following the same idea, a similar decomposition of the stress is proposed here but in a more general way. A more general "viscous inducing" part of the stress tensor is now considered. Therefore, this part of the stress tensor contains also viscoelastic inducing effects. Accordingly, the stresses can be written as

$$\boldsymbol{\sigma} = \boldsymbol{\sigma}_{\text{e,reac}} + \boldsymbol{\sigma}_{\text{v,ind}}, \tag{17}$$

where the subscript e,reac refers to the "elastic reaction" part and the subscript v,ind to the "viscous inducing" part of the stresses. In other words, the inducing part of the stresses depends on the strain rate and lead to a viscoelastic-viscoplastic response. Kaliske and Rothert (1997) have reported that the viscoelastic behaviour is, mainly linked to the isochoric part of the deformation, which excludes the hydrostatic pressure contribution. In the present model, viscoelasticity is considered independent of the hydrostatic pressure in the polymeric matrix. In addition, the behaviour of the fibres is assumed to be purely elastic. The same hypothesis are used in the previous viscoplastic model but for the viscoplastic contribution. This allows the definition of the same "viscous inducing" part of the stresses for both the viscoelastic and the viscoplastic behaviour. Consequently, the different parts of the stresses are expressed as follows

$$\boldsymbol{\sigma}_{\text{e,reac}} = p\boldsymbol{I} + \sigma_f \boldsymbol{A}, \tag{18}$$

$$\boldsymbol{\sigma}_{\text{v,ind}} = \boldsymbol{\sigma} - \boldsymbol{\sigma}_{\text{e,reac}} = \boldsymbol{s}, \tag{19}$$

where the term $\sigma_f \boldsymbol{A}$ corresponds to the stress projected in the fibre direction, i.e. the fibre contribution to the stress, and the terms $\boldsymbol{s}$ and $p\boldsymbol{I}$ are the deviatoric part and the hydrostatic pressure of the stress in the matrix only. The scalars p and σ_f are determined by imposing the following conditions

$$\boldsymbol{s} : \boldsymbol{I} = 0 \quad \text{and} \quad \boldsymbol{s} : \boldsymbol{A} = 0. \tag{20}$$

These conditions correspond to a trace of the deviatoric part equal to zero and no contribution of the fibre direction, leading to the following expressions for p and σ_f

$$p = \frac{1}{2}(\boldsymbol{\sigma} : \boldsymbol{I} - \boldsymbol{\sigma} : \boldsymbol{A}), \quad \text{and} \quad \sigma_f = \frac{1}{2}(3\,\boldsymbol{\sigma} : \boldsymbol{A} - \boldsymbol{\sigma} : \boldsymbol{I}). \tag{21}$$

Introducing Eqs. (21) in Eq. (19) leads to the direct relationship between the total stresses and the "viscous inducing" part of the stresses

$$\boldsymbol{\sigma}_{\text{v,ind}} = \mathbb{P}_{\text{v,ind}} : \boldsymbol{\sigma}, \tag{22}$$

with

$$\mathbb{P}_{\text{v,ind}} = \mathbb{I} - \frac{1}{2}\boldsymbol{I} \otimes \boldsymbol{I} - \frac{3}{2}\boldsymbol{A} \otimes \boldsymbol{A} + \frac{1}{2}(\boldsymbol{A} \otimes \boldsymbol{I} + \boldsymbol{I} \otimes \boldsymbol{A}). \tag{23}$$

The $\mathbb{P}_{\text{v,ind}}$ tensor is identified as the fourth order operator that is used to identify, the components of the stress tensor that affect the viscous response, i.e. shear in the polymeric matrix, and to remove the components that do not depend on the strain-rate.

Considering the isotropic material behaviour of the polymer, an alternative approach is proposed to obtain the fourth order tensor $\mathbb{\Gamma}_1$, using the previous stress decomposition. The approach consists in using one single scalar as a viscoelastic parameter, $\gamma_{ve,1}$, as for an isotropic material, and the $\mathbb{P}_{\text{v,ind}}$ tensor for the definition of $\mathbb{\Gamma}_1$. The resulting expression of $\mathbb{\Gamma}_1$ is then

$$\mathbb{\Gamma}_1 = \gamma_{\text{ve,1}} \mathbb{P}_{\text{v,ind}}. \tag{24}$$

In the last equation, the parameter $\gamma_{ve,1}$ is the viscoelastic parameter that quantifies the viscous effect, while the fourth order tensor $\mathbb{P}_{\text{v,ind}}$ provides the direction of the viscoelastic evolution. With the proposed approach, the number of parameters that need to be identified is significantly reduced: the full identification of the

viscoelastic model uses only two scalar parameters, τ_1 and $\gamma_{\text{ve},1}$. Moreover, the proposed extension remains in the framework of the invariant theory previously formulated, in order to keep the benefits of this formulation.

The defined "viscous inducing" stresses are considered to formulate the viscoplastic creep surface using the invariant theory. The set of invariants that are used in the model are the following

$$\begin{aligned} \mathrm{I}_1 &= \frac{1}{2}\,\mathrm{tr}(\boldsymbol{\sigma}^2_{\text{v,ind}}) - \underline{a}\,(\boldsymbol{\sigma}^2_{\text{v,ind}})\,\underline{a}, \\ \mathrm{I}_2 &= \underline{a}\,(\boldsymbol{\sigma}^2_{\text{v,ind}})\,\underline{a}, \\ \mathrm{I}_3 &= \mathrm{tr}(\boldsymbol{\sigma}) \;-\; \underline{a}\,\boldsymbol{\sigma}_{\text{v,ind}}\,\underline{a}, \end{aligned} \tag{25}$$

with

$$\boldsymbol{\sigma}^2_{\text{v,ind}} = \boldsymbol{\sigma}_{\text{v,ind}} \cdot \boldsymbol{\sigma}_{\text{v,ind}}. \tag{26}$$

The corresponding transversely isotropic viscoplastic creep surface for UD composites reads

$$f(\boldsymbol{\sigma}, \bar{\varepsilon}_{\text{vp}}, \boldsymbol{A}) = \alpha_1 \mathrm{I}_1 + \alpha_2 \mathrm{I}_2 + \alpha_3 \mathrm{I}_3 + \alpha_{32} \mathrm{I}_3^2 - 1 \leq 0, \tag{27}$$

where

$$\begin{aligned} &\alpha_3 = \alpha_3^t \quad \alpha_{32} = \alpha_{32}^t \quad \text{if} \quad \mathrm{I}_3 > 0, \\ &\alpha_3 = \alpha_3^c \quad \alpha_{32} = \alpha_{32}^c \quad \text{if} \quad \mathrm{I}_3 \leq 0, \end{aligned} \tag{28}$$

and the equivalent viscoplastic strain is defined as

$$\bar{\varepsilon}_{\text{vp}} = \sqrt{\frac{1}{2}(\boldsymbol{\varepsilon}_{\text{vp}})_{ij}(\boldsymbol{\varepsilon}_{\text{vp}})_{ij}}. \tag{29}$$

The proposed viscoplastic creep function is formulated using six viscoplastic creep α-parameters. They must be determined using the hardening data of the

material in six different loading scenarios. These scenarios are: transverse shear, in-plane shear, uniaxial and biaxial transverse tension and uniaxial and biaxial transverse compression. Fig. 2 shows a schematic representation of the transversely isotropic f surface in stress space. The displayed points are the "trigger points" of the viscoplastic creep surface, for a given strain rate and a given plastic strain, in which the plastic yield stress value is known thanks to the tabulated hardening data, given as an input parameter of the model. Therefore, the viscoplastic creep surface parameters $\alpha_{(...)}$ are a function of the strain rate Koerber et al. (2010) and of the plastic strain Vogler et al. (2013).

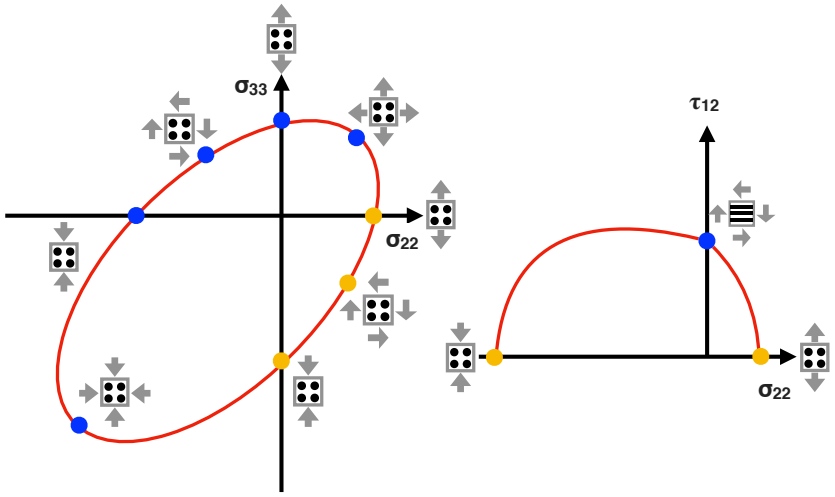

Figure 2: Schematic representation of the yield surface for UD composites in stress space (the yellow points are repetitions of the blue ones because of the material symmetry).

The evolution of the viscoplastic strain is defined by using a non-associative flow rule. Two viscous parameters define the Perzyna (see Perzyna (1963)) type overstress model, m a dimensionless exponent parameter to be definded accordingly to the material type and η the viscosity parameter, which has the unit Ns/mm^2.

A non-negative parameter, known as the consistency parameter, $\dot{\gamma}_{\text{vp}}$, is to be determined for the flow rule, which reads

$$\dot{\boldsymbol{\varepsilon}}_{\text{vp}} = \dot{\gamma}_{\text{vp}} \boldsymbol{n}_{\text{g}} = \frac{\langle f^m(\boldsymbol{\sigma}, \bar{\varepsilon}_{\text{vp}}, \boldsymbol{A}) \rangle}{\eta} \boldsymbol{n}_{\text{g}}, \tag{30}$$

where $\boldsymbol{n}_{\text{g}} = \partial_{\boldsymbol{\sigma}} \text{g}(\boldsymbol{\sigma}, \boldsymbol{A})$ is the non-associated viscoplastic flow direction, analogous to plasticity. The viscoplastic potential function is defined as

$$\text{g}(\boldsymbol{\sigma}, \boldsymbol{A}) = \beta_1 I_1 + \beta_2 I_2 + \beta_3 I_3^2 - 1. \tag{31}$$

It uses the same invariants as the viscoplastic creep function $f(\boldsymbol{\sigma}, \bar{\varepsilon}_{\text{vp}}, \boldsymbol{A})$ and the β-parameters are determined for the material using the procedure described by Vogler et al. (2013). The viscoplastic potential can be directly expressed using the stresses as

$$\text{g}(\boldsymbol{\sigma}, \boldsymbol{A}) = \frac{1}{2} \boldsymbol{\sigma} : \mathbb{M} : \boldsymbol{\sigma} + \boldsymbol{N} : \boldsymbol{\sigma} - 1, \tag{32}$$

where $\mathbb{M}$ and $\boldsymbol{N}$ are expressed using the β-parameters and the structural tensors. The viscosity parameter acts as delay parameter, activating the viscous behaviour for high strain rates. The time discretisation transforms Eq. (30) into

$$\frac{\Delta \boldsymbol{\varepsilon}_{\text{vp}}^{n+1}}{\Delta t^{n+1}} = \frac{\Delta \gamma_{\text{vp}}^{n+1}}{\Delta t^{n+1}} \boldsymbol{n}_{\text{g}}. \tag{33}$$

This discretised flow rule results in the criterion that is used to verify wether the evolution is purely viscoelastic or not. This criterion reads

$$f(\boldsymbol{\sigma}^{\text{pred},n+1}, \bar{\varepsilon}_{\text{vp}}^{n+1}, \boldsymbol{A}) < 0. \tag{34}$$

If the criterion is satisfied, then the evolution is purely viscoelastic and the predicted stresses are correct. Otherwise, there is a viscoplastic evolution, and both the viscoplastic strains and the stresses must be computed. The total stresses read

$$\boldsymbol{\sigma}^{n+1} = \boldsymbol{\sigma}^{\text{pred},n+1} - \mathbb{C}_{ve}^{n+1} : \Delta \boldsymbol{\varepsilon}_{\text{vp}}^{n+1}, \tag{35}$$

with

$$\Delta\boldsymbol{\varepsilon}_{\text{vp}}^{n+1} = \Delta\gamma_{\text{vp}}^{n+1}\ (\mathbb{M} : \boldsymbol{\sigma}^{n+1} + \boldsymbol{N}), \tag{36}$$

according to Eq. (33). The following expression of $\boldsymbol{n}_{\text{g}}$ in terms of tensors is used

$$\boldsymbol{n}_{\text{g}} = \mathbb{M} : \boldsymbol{\sigma}^{n+1} + \boldsymbol{N}. \tag{37}$$

Then, the following expression of the stresses as a function of γ_{vp}^{n+1} is obtained

$$\boldsymbol{\sigma}^{n+1} = \mathbb{F}^{-1} : (\boldsymbol{\sigma}^{\text{pred},n+1} - \Delta\gamma_{\text{vp}}^{n+1}\ \mathbb{C}_{ve}^{n+1} : \boldsymbol{N}), \tag{38}$$

with

$$\mathbb{F} = \mathbb{I} + \Delta\gamma_{\text{vp}}^{n+1}\ \mathbb{C}_{ve}^{n+1} : \mathbb{M} \tag{39}$$

The expression of the stresses (see Eq. (38)) is introduced in Eq. (34), which is solved using a local Newton-Raphson algorithm to obtain the value of the consistency parameter $\Delta\gamma_{\text{vp}}^{n+1}$. Indeed, as the stresses are only function of $\Delta\gamma_{\text{vp}}^{n+1}$, the viscoplastic creep function f at $t = t^{n+1}$ can be written as a function of $\Delta\gamma_{\text{vp}}^{n+1}$ only making it the only variable to be determined. The residual reads at the local step (k)

$$R_f^{n+1}|^{(k)} = \langle f^m(\Delta\gamma_{\text{vp}}^{n+1}|^{(k)})\rangle - \eta\ \frac{\Delta\gamma_{\text{vp}}^{n+1}|^{(k)}}{\Delta t^{n+1}}. \tag{40}$$

It is linearised and gives the value of the local increment $\Delta^2\gamma_{\text{vp}}^{n+1}|^{(k)} = \Delta\gamma_{\text{vp}}^{n+1}|^{(k+1)} - \Delta\gamma_{\text{vp}}^{n+1}|^{(k)}$

$$\Delta^2\gamma_{\text{vp}}^{n+1}|^{(k)} = -\frac{R_f^{n+1}|^{(k)}}{\dfrac{\partial R_f^{n+1}|^{(k)}}{\partial\gamma_{\text{vp}}^{n+1}|^{(k)}}}, \tag{41}$$

with

$$\frac{\partial R_f^{n+1}|^{(k)}}{\partial \Delta\gamma_{\text{vp}}^{n+1}|^{(k)}} = \frac{\partial (f^m - \eta[\Delta\gamma_{\text{vp}}^{n+1}|^{(k)}/\Delta t^{n+1}])}{\partial \Delta\gamma_{\text{vp}}^{n+1}|^{(k)}} \tag{42}$$

$$= m\, f^{m-1}[\partial f/\partial \Delta\gamma_{\text{vp}}^{n+1}|^{(k)}] - [\eta/\Delta t^{n+1}]. \tag{43}$$

The local Newton-Raphson algorithm stops when the prescribed tolerance parameter is achieved for the residual, i. e. $R_f^{n+1} \leq$ tolerance. Then, the viscoplastic strains $\boldsymbol{\varepsilon}_{\text{vp}}^{n+1}$ can be updated at the end of the current time step.

A schematic representation of the described constitutive model implementation through a VUMAT user subroutine is presented in Fig. 3.

3. Calibration of the viscous parameters

It is assumed that the viscoelastic behaviour is independent of the hydrostatic pressure. Hence, the strain rate dependency on the yielding behaviour and on the elastic behaviour is similar both in tension and in compression. The finite element simulations used in the calibration process are done with specimens and boundary conditions identical to those presented in Sec. 4.1. The calibrated parameters are summarised in table 2.

3.1. Calibration of the viscoelastic model parameters

The identification of the two viscoelastic parameters τ_1 and $\gamma_{\text{ve},1}$ of the proposed viscoelastic model, introduced in Eq. (12) and (24), is based on the $90°$ compression tests. Indeed, under transverse solicitations, the response is rate-dependent and controlled by the matrix. Currently, it is easier to calibrate the viscoelastic response caused by the matrix using this case. The $45°$ tests are used

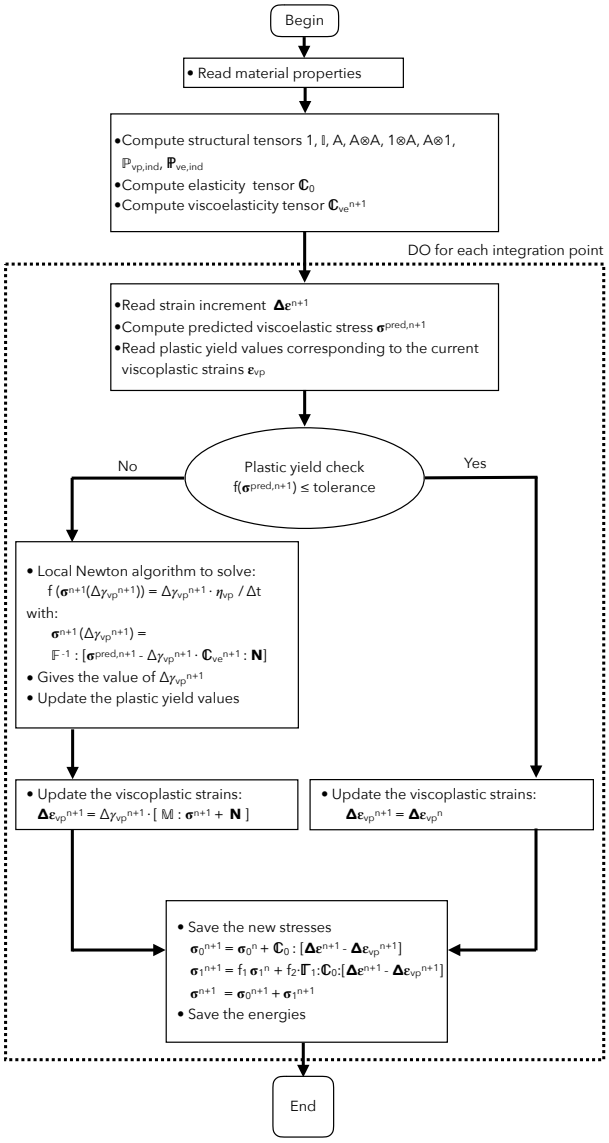

Figure 3: schematic representation of the proposed model implemented in the VUMAT

to control the validity of the model under shear loading but are less sensible to the value of $\gamma_{ve,1}$ so they cannot be used independently. Approximated values are obtained using a 1D calculation, and then refined using a finite element simula-

tion with a fine mesh, reproducing the experimental conditions. Only two strain-rate regimes are available, therefore there is some uncertainty for the value of τ_1. Indeed, no noticeable difference is observed for values in the range of 10^{-1} to 10^{-4} s. This parameter controls the value of a strain rate threshold, below which no noticeable strain rate effect would be noticeable. It is to be adjusted with more experimental data. Here, τ_1 is set to $\tau_1 = 1 \cdot 10^{-2}$ s and the value $\gamma_{\text{ve},1} = 0.32$ is found for the best approximation.

3.2. Calibration of the viscoplastic model parameters

The calibration of the two viscoplastic parameters, m and η, introduced in Eq. (30) is discussed herein. For the current material, IM7-8552, only two loading speeds are available. Consequently, the parameter m is set to $m = 1$, which leads to an approximately linear dependency of the viscoplastic yield stress on the logarithmic strain rate. Schaefer et al. (2014) reported the existence of such a dependency for carbon-epoxy systems. However, thermoplastic toughened resins exhibit a nonlinear dependency on the logarithmic strain rate Vogler (2012). Therefore, the parameter m can be modified in the model to fit to one material or the other. In the case of such a nonlinear dependency on the logarithmic strain rate, test data for at least 3 strain rate regimes are needed to calibrate the parameter m.

To calibrate the remaining viscoplastic parameter η, the axial true stress-true strain curves of the 45° off-axis compression tests are used. These tests were performed at two different strain rates, at a quasi-static strain rate of 0.0004 s^{-1}, and at a dynamic axial strain rate, with an approximate value of 280 s^{-1} (see Koerber et al. (2010, 2018)). The calibration is first performed by running simulations on a single element mesh and followed by simulation using a fine mesh, whereby the parameter $\eta = 3.5 \cdot 10^{-4}$ Ns/mm^2 gives the best approximation.

Parameter name	Value	Unit
m	1	$-$
η	$3.5 \cdot 10^{-4}$	Ns/mm^2
τ_1	$1 \cdot 10^{-2}$	s
$\gamma_{\text{ve},1}$	0.32	$-$

Table 2: Viscous parameters after calibration for the material system Hexcel® IM7-8552

4. Results

The numerical results are presented in this section and compared to the experimental results. As the model is implemented as a VUMAT, the integration scheme is explicit. In such a scheme, the time stable increment during one step is very small in order to ensure the stability of the simulation. This time stable increment depends mostly on the elements size and on the mass of these elements, i.e. their material's density. Consequently, for the same mesh and the same density, the quasi-static and dynamic simulations have the same stable time increment value. As the simulations are given a total loading duration, the number of increment will be the ratio between this duration and the time stable increment. This can be a problem for the quasi-static loading cases, as the loading duration is approximately 30 seconds, while it is only approximately 10^{-4}s for the dynamic loading cases. Indeed, running a quasi-static prediction would then require 10^5 times more increments than running a dynamic one. It would result in a total CPU time far too high for the model to be efficient in the case of very low-speed loading cases. A way to deal with it is to use mass scaling. By changing the material density, it

is possible to increase the value of the stable time increment. Here, the density of the material is multiplied by a factor 10^6 for the quasi-static simulations. By doing this, the time stable increment is multiplied by the square root value of this factor, which means here by 1000, so the number of increments needed is divided by 1000. In the end, approximately 100 times more increments are needed to run a quasi-static simulation, so the model can be relevant to simulate this type of loading case. A verification of the ratio kinetic energy/internal energy, done at the end of the simulation, shows that this mass scaling has a negligible effect on the final result. The ratio never exceed more than $0.4\ \%$ with mass scaling, compared to $4 \cdot 10^{-4}\ \%$ without it, and no effect on the predictions was observed.

4.1. Boundary conditions and meshes

The simulations are performed using the finite element commercial software Abaqus. The experimental specimens are reproduced using three-dimensional, eight-node C3D8R solid elements with reduced integration. For low strain rate simulations, the viscoelasticity transforms into pure linear elasticity. Consequently, the element size effect on the results is very small. However, it is more important to refine the mesh under high strain rates because all areas in the specimen do not necessarily deform at the same speed. For these reasons, the following results have been obtained using a coarse mesh for the quasi-static simulations, and a fine mesh for the dynamic simulations, for which the hourglass effect was investigated and not detected. A single element mesh has also been tested, as it provides a very efficient simulation without compromising the accuracy. The meshes used for the compression simulations are represented in Fig. 4. The meshes used for the tension simulations are different because the specimens have different dimensions, but the element sizes are similar.

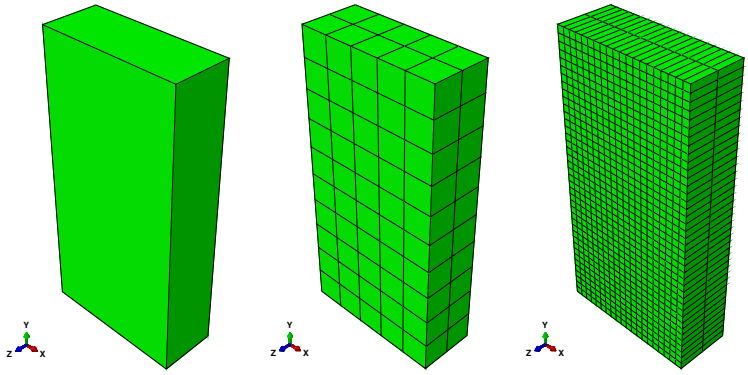

Figure 4: Meshes used for the compressive load simulation, a single element, a coarse, and a fine mesh

The applied boundary conditions are represented in Fig. 5 and correspond to the experimental testing boundary conditions for both tensile and compression loading cases. To replicate the experimental tests, a displacement boundary condition was applied on one of the ends of the specimen.

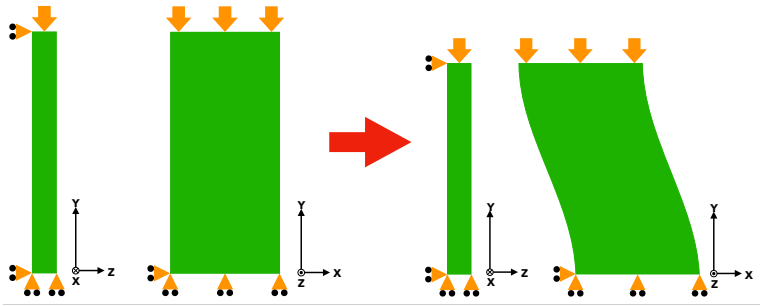

Figure 5: Boundary conditions for the compression loading simulations

The simulated cases are off-axis $15°$, $30°$, $45°$ and $90°$ transverse tension and off-axis $15°$, $30°$, $45°$, $60°$, $75°$ and $90°$ transverse compression.

The experimental and simulated axial true strain–true stress curves are plotted

in Figs 6–15, for dynamic and quasi-static regimes, for both tension and compression. The tolerance in the local Newton-Raphson algorithm is fixed at 10^{-10}, and its effect is studied further in the paper. The dotted lines refer to the dynamic data, the continuous lines refer to the quasi-static data. Also, the red colour is used for the simulation results, while the black colour is used for the experimental results. Note that, the damage and the failure are not taken into account in the current model, and no information about damage in the test specimens was available.

4.2. Tension results

The method used to read the axial stress and strain in the specimen in the simulation is the same for all the specimens. The axial true strain, computed using the value of the axial displacement of the free extremity of the specimen reads

$$\varepsilon_{axial} = \mathrm{Log}\Big(1 + \frac{\Delta l}{l_0}\Big) = \mathrm{Log}\Big(\frac{l}{l_0}\Big). \tag{44}$$

The axial stress is then computed by reading the sum of the reaction forces at the end of the specimen, P, and using the value of the axial strain and the initial section as follows

$$\sigma_{axial} = \frac{P}{A_0}\Big(1 + \frac{l}{l_0}\Big), \tag{45}$$

In Eq. (45), the hypothesis of incompressibility is applied to estimate the current cross section. This condition reads:

$$A = A_0\frac{l_0}{l} = A_0\Big(1 + \frac{\Delta l}{l_0}\Big)^{-1} \tag{46}$$

This condition is used here because it was used to obtain the experimental curves (see Koerber et al. (2018)). By doing so, the same quantities are read in both

simulations and experiments. The Figs. 6–9 show the measured and simulated static and dynamic axial true stress-true strain curves under 15°, 30°, 45° off-axis tension and 90° transverse tension. Considering the experimental data of the dynamic tests, it can be seen that with a higher strain rate the initial slope increases. This means that viscous effects are observed in the elastic range and these must be taken into account. The model proposed is able to provide a good accuracy in the prediction of these effects. Also, the true stress-true strain curves become more linear under dynamic loading, delaying the onset of plasticity (See Figs. 6-9). This observation is in agreement with the viscoelastic-viscoplastic behaviour of the material which is modelled here. In that respect, the viscous effects noticed in both, elastic and plastic ranges, are very accurately predicted for the four orientations. It is therefore concluded that the model is valid for tensile simulations.

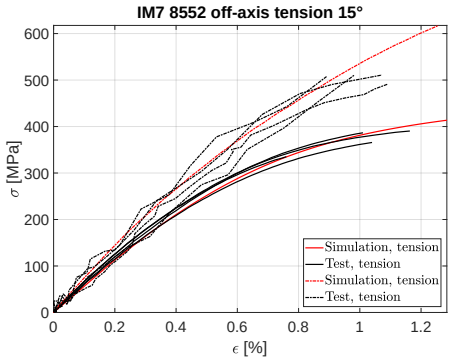

Figure 6: Axial true stress-true strain curves for the tensile tests and simulations, 15°.

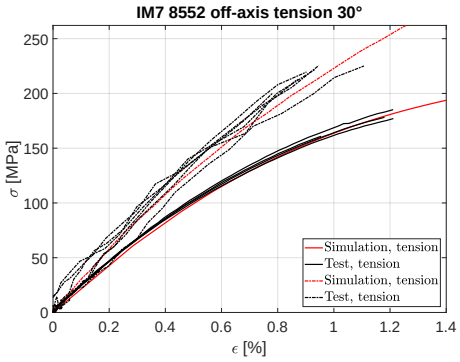

Figure 7: Axial true stress-true strain curves for the tensile tests and simulations, 30°.

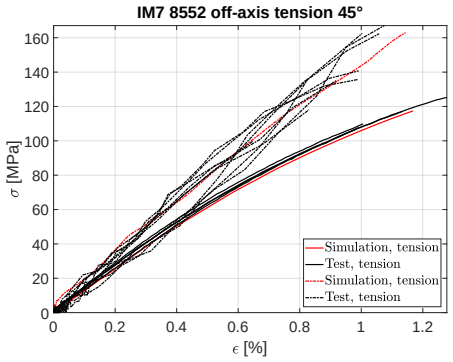

Figure 8: Axial true stress-true strain curves for the tensile tests and simulations, 45°.

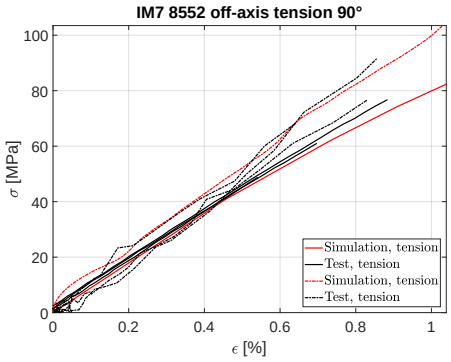

Figure 9: Axial true stress-true strain curves for the tensile tests and simulations, 90°.

4.3. Compression results

The Figs. 10–15 show the measured and predicted axial true stress-true strain curves for 15°, 30°, 45°, 60°, 75° off-axis compression and 90° transverse compression under quasi-static and dynamic loadings. As can be observed, a good prediction of the nonlinear behaviour was achieved for both quasi-static and dynamic loading cases. For compression loadings as well as tensile loadings, the viscous effects are properly taken into account by the model proposed here. Nevertheless, it showed be noted that for the 15°, 30°, 45° off-axis dynamic compression, the last part of the experimental curves i.e. the plateau cannot be fully reproduced. Indeed, the model does not consider damage in the material, and the evolution observed could result from macroscopic damage. No experimental investigation of the damage mechanisms was performed so this remains a hypothesis. A more thorough viscoplastic damage model could improve the predictions for those specimens.

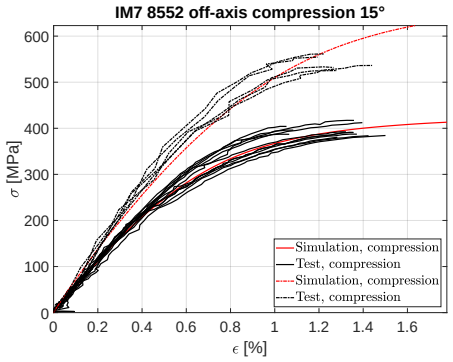

Figure 10: Axial true stress-true strain for the compression tests and simulations, 15°.

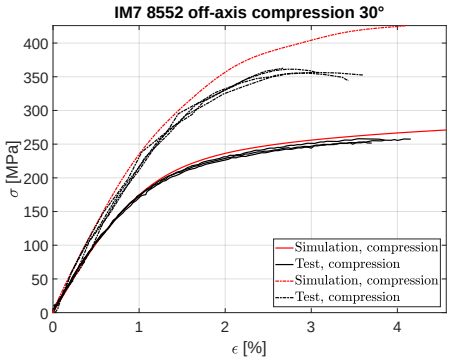

Figure 11: Axial true stress-true strain curves for the compression tests and simulations, 30°.

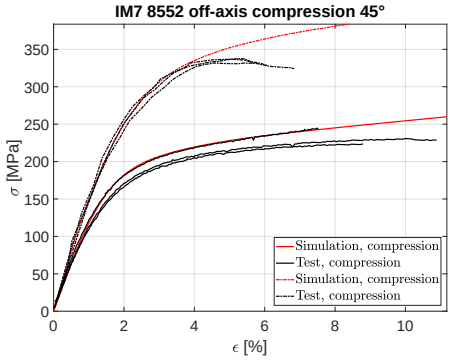

Figure 12: Axial true stress-true strain curves for the compression tests and simulations, 45°.

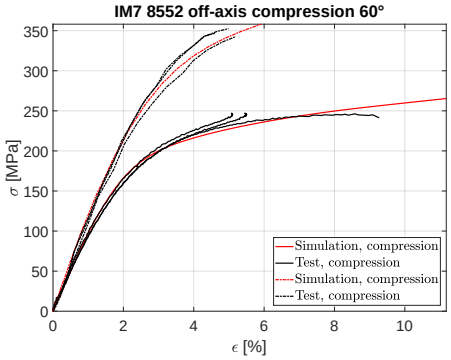

Figure 13: Axial true stress-true strain curves for the compression tests and simulations, 60°.

5. Model efficiency

In this section, an analysis of the calculation efficiency is presented. The computation time in different scenarios is compared for the former elastic-plastic Vogler et al. (2013) and elastic-viscoplastic Koerber et al. (2018) model and the presented viscoelastic-viscoplastic model. The influence of the criterion's value in the local Newton-Raphson algorithm in the viscoplastic part is also discussed.

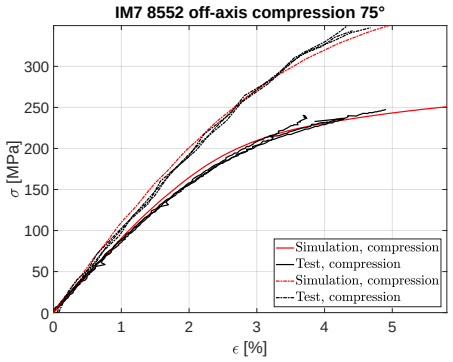

Figure 14: Axial true stress-true strain curves for the compression tests and simulations, 75°.

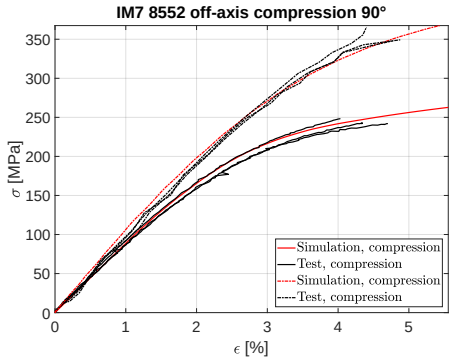

Figure 15: Axial true stress-true strain curves for the compression tests and simulations, 90°.

5.1. Comparison in term of computation time between the present model and its predecessors

A comparison of the three successive models, which are successively, elastic-plastic, elastic-viscoplastic, and the presented viscoelastic-viscoelastic model, is shown in Fig. 16 and 17. It should be noted that no scaling functions for the elastic properties, such as those proposed in Koerber et al. (2018), were used in the simulations. The quasi-static simulations were performed using a coarse mesh, while a finer mesh was used in the dynamic case. As expected, the three simulated curves for the quasi-static simulations are the same, the viscous effects being inexistent at that speed. However, a noticeable difference exists between the models in the dynamic loading case, where the viscous effects in the elastic part are well represented by the current model. Evidently, the elastic-plastic model cannot give an accurate prediction for a dynamic loading case, as the formulation is not strain rate-dependent. The CPU times required for each of the simulation cases, i.e. dynamic/quasi-static and fine/coarse mesh, are plotted in Fig. 18, in the case of a 45° off-axis compression loading. As can be seen, the total CPU times are

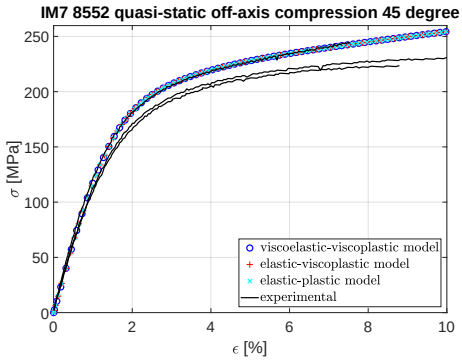

Figure 16: Axial true stress-true strain curves for the quasi-static 45° off-axis compression, simulations and experiments.

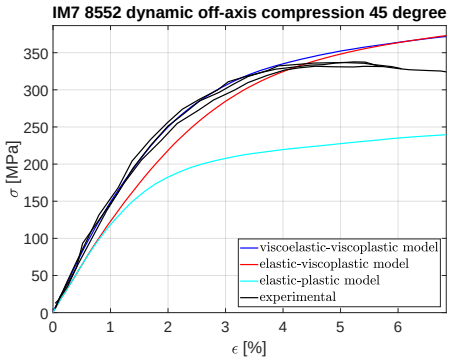

Figure 17: Axial true stress-true strain curves for the dynamic 45° off-axis compression, simulations and experiments.

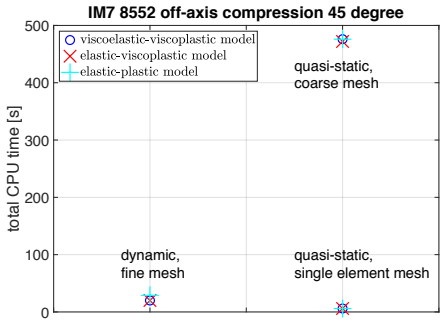

Figure 18: Comparison of the total CPU time between the successive models.

very similar between the different models. The present viscoelastic-viscoplastic model provides more accurate results without any loss in the efficiency. In summary, it can be concluded that the new model accounts for viscous effects in both the elastic and the plastic range without any supplementary computational cost.

5.2. *Influence of the tolerance's value in the local Newton-Raphson algorithm in the viscoplastic part*

Another study concerning the efficiency of the proposed model is presented in this section. Here, the influence of the value of the tolerance parameter in the local Newton-Raphson algorithm, on both the total CPU time and the accuracy of the prediction, is shown. In Fig. 19 can be seen the evolution of the total CPU time, in the case of 45° off-axis compression, as a function of the tolerance. The dynamic simulations were performed using the finer mesh while a coarse mesh is used for the quasi-static predictions. The influence is almost unnoticeable

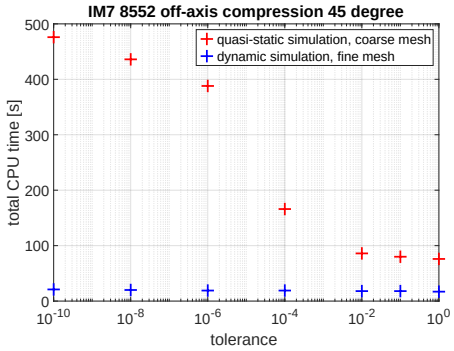

Figure 19: Evolution of the total CPU time as a function of the tolerance parameter.

for the dynamic predictions, as they do not require more than 20 seconds to be performed. Indeed, there are few increments because of the very short loading duration. However, the evolution is very important in the case of the quasi-static simulations. With a value of 10^{-10} for the tolerance, the total CPU time is almost eights minutes and drops to less than two minutes for a value $\leq 10^{-2}$. By doing this, the computation time is divided by four, which is far from being negligible. It must be then assessed that such an increase of the tolerance's value is without consequences on the quality of the predictions. Fig. 20 and 21 show the influence

of varying the tolerance's value regarding the prediction quality, in both quasi-static and dynamic loading cases. It can be noticed that for values above 10^{-2},

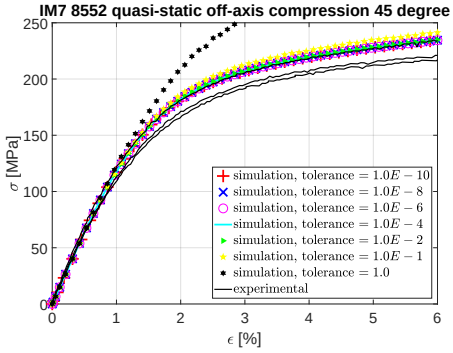

Figure 20: Axial true stress-true strain curves for the quasi-static 45° off-axis compression, with varying the tolerance's value.

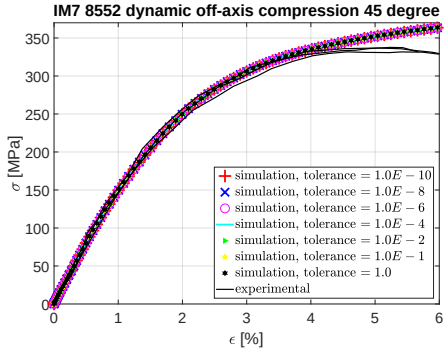

Figure 21: Axial true stress-true strain curves for the dynamic 45° off-axis compression, with varying the tolerance's value.

the quality of the prediction is degraded for the quasi-static loading case, and for a tolerance of one, the predictions show premature divergence. For the dynamic loading case, however, no difference is observed, even for a value of one for the tolerance the prediction remains unchanged, all the curves are exactly similar. Therefore, a value of 10^{-2} for the tolerance seems to be ideal to both improve the efficiency of the model and preserving its accuracy. This value is then tested for all the loading cases, i.e. dynamic/quasi-static regimes and compression/tensile loadings, and proves fully satisfying. It allows a drastic increase of the model performance when compared to the initial value of 10^{-10}.

6. Conclusion

A fully 3D viscoelastic-viscoplastic model was proposed. The viscoelastic formulation, expressed within the framework of the invariant theory, along with

the changes that accompany it, were explained in detail. The model accuracy in predicting the axial true stress-true strain behaviour was assessed for the material system Hexcel® IM7-8552. The quality of the predictions is remarkably good. A comparison between the capabilities and efficiency of the present model and its predecessors was also investigated. The present model correctly fills the lack of its predecessor in term of predicting the viscous effects in the elastic range. These effects are of primordial importance, as for the proper calibration of the viscoplastic part, and for the simulation of complex loading scenarios. Moreover, no loss in the model's efficiency that could be a handicap for further development is observed.

As the model works at the laminate scale, one specimen can be modelled using only one element in a finite element algorithm, and still provide accurate results in a very short time. This makes the model relevant to the domain of designing and optimising structural parts at the meso-scale. Furthermore, the calibration can be done quickly for any UD composite material thanks to the limited number of material properties required.

ACKNOWLEDGEMENTS

The second and third authors gratefully acknowledge the funding of Project NORTE-01-0145-FEDER-000022 SciTech Science and Technology for Competitive and Sustainable Industries, co-financed by Programa Operacional Regional do Norte (NORTE2020), through Fundo Europeu de Desenvolvimento Regional (FEDER).

The last author gratefully acknowledges the funding of Project PTDC/EMS-PRO/4732/2014, co-financed by Programa Operacional Competitividade e Interna-

cionalização.

References

Chen, J.L., Sun, C.T., 1993. A Plastic Potential Function Suitable for Anisotropic Fiber Composites. J. Compos. Mater. 27, 1379–1390. doi:10.1177/002199839302701403.

Dassault Systèmes, . ABAQUS EXPLICIT 2017. URL: https://www.3ds.com/products-services/simulia/products/abaqus/abaqusexplicit/.

El-Qoubaa, Z., Othman, R., 2015. Characterization and modeling of the strain rate sensitivity of polyetheretherketone's compressive yield stress. Mater. Des. 66, 336–345. doi:10.1016/j.matdes.2014.10.080.

El-Qoubaa, Z., Othman, R., 2016. Strain rate sensitivity of polyetheretherketone's compressive yield stress at low and high temperatures. Mech. Mater. 95, 15–27. doi:10.1016/j.mechmat.2015.12.008.

Gao, S.L., Kim, J.K., 2000. Cooling rate influences in carbon fibre/PEEK composites. Part I: Crystallinity and interface adhesion. Compos. Part A Appl. Sci. Manuf. 31, 517–530. doi:10.1016/S1359-835X(00)00009-9.

Garcia-Gonzalez, D., Zaera, R., Arias, A., 2017. A hyperelastic-thermoviscoplastic constitutive model for semi-crystalline polymers: Application to PEEK under dynamic loading conditions. Int. J. Plast. 88, 27–52. doi:10.1016/j.ijplas.2016.09.011.

Gates, T.S., Sun, C.T., 1991. Elastic/Viscoplastic Constitutive Model for Fiber Reinforced Thermoplastic Composites. AIAA J. 29, 457–463. doi:10.2514/3.59922.

Gerbaud, P.W., Otero, F., Bussetta, P., Camanho, P.P., 2018. Viscoelastic-viscoplastic constitutive model for unidirectional fibre reinforced polymers, in: 6th European Conference on Computational Mechanics, Glasgow, 11–15 June 2018.

Jar, P.Y.B., Kausch, H.H., 1994. The influence of moulding conditions on delamination behaviour of carbon-fibre/peek composites. Compos. Sci. Technol. 52, 349–359. doi:10.1016/0266-3538(94)90169-4.

Kaliske, M., 2000. A formulation of elasticity and viscoelasticity for fibre reinforced material at small and finite strains. Comput. Methods Appl. Mech. Eng. 185, 225–243. doi:10.1016/S0045-7825(99)00261-3.

Kaliske, M., Rothert, H., 1997. Formulation and implementation of three-dimensional viscoelasticity at small and finite strains. Comput. Mech. 19, 228–239. doi:10.1007/s004660050171.

Koerber, H., Kuhn, P., Ploeckl, M., Otero, F., Gerbaud, P.W., Rolfes, R., Camanho, P.P., 2018. Experimental characterization and constitutive modeling of the non-linear stress–strain behavior of unidirectional carbon–epoxy under high strain rate loading. Advanced Modeling and Simulation in Engineering Sciences 5, 17. doi:10.1186/s40323-018-0111-x.

Koerber, H., Xavier, J., Camanho, P.P., 2010. High strain rate characterisation of unidirectional carbon-epoxy IM7-8552 in transverse compression and in-plane

shear using digital image correlation. Mech. Mater. 42, 1004–1019. doi:10.1016/j.mechmat.2010.09.003.

Kuhn, P., Ploeckl, M., Koerber, H., 2015. Experimental investigation of the failure envelope of unidirectional carbon-epoxy composite under high strain rate transverse and off-axis tensile loading. EPJ Web Conf. 94, 01040. doi:10.1051/epjconf/20159401040.

Perzyna, P., 1963. Constitutive equations for rate-sensitive plastic materials. Q. Appl. Math. 20, 321–331. doi:10.2307/43636430.

Poon, H., Ahmad, M.F., 1998. A material point time integration procedure for anisotropic, thermo rheologically simple, viscoelastic solids. Comput. Mech. 21, 236–242. doi:10.1007/s004660050298.

Rae, P.J., Brown, E.N., Orler, E.B., 2007. The mechanical properties of poly(ether-ether-ketone) (PEEK) with emphasis on the large compressive strain response. Polymer (Guildf). 48, 598–615. doi:10.1016/j.polymer.2006.11.032.

Schaefer, J.D., Werner, B.T., Daniel, I.M., 2014. Strain-Rate-Dependent Failure of a Toughened Matrix Composite. Exp. Mech. 54, 1111–1120. doi:10.1007/s11340-014-9876-0.

Sun, C.T., Chen, J.L., 1989. A Simple Flow Rule for Characterizing Nonlinear Behavior of Fiber Composites. J. Compos. Mater. 23, 1009–1020. doi:10.1177/002199838902301004.

Vaziri, R., Olson, M.D., Anderson, D.L., 1991. A Plasticity-Based Constitutive

Model for Fibre-Reinforced Composite Laminates. J. Compos. Mater. 25, 512–535. doi:10.1177/002199839102500503.

Vogler, M., 2012. Anisotropic Material Models for Fiber Reinforced Polymeres. Ph.D. thesis. Leibniz Universität Hannover.

Vogler, M., Koerber, H., Kuhn, P., Rolfes, R., Camanho, P.P., 2015. Constitutive Modeling and Experimental Characterization of the Non-Linear Stress-Strain Behavior of Unidirectional Carbon-Epoxy Under High High Strain Rates, in: 20th International Conference on Composite Materials, Copenhagen, 19–24 July 2015.

Vogler, M., Rolfes, R., Camanho, P.P., 2013. Modeling the inelastic deformation and fracture of polymer composites-Part I: Plasticity model. Mech. Mater. 59, 50–64. doi:10.1016/j.mechmat.2012.12.002.